AD-A033 854 NAVAL RESEARCH LAB WASHINGTON D C F/G 4/1

PARAMETERIZATION OF THE ATMOSPHERIC HEATING RATE FROM 15 TO 120--ETC(U)

NOV 76 D F STROBEL

UNCLASSIFIED NRL-MR-3398 NL

| OF |

AD
A033854

END

DATE
FILMED
2-77

NRL Memorandum Report 3398

Parameterization of the Atmospheric Heating Rate from 15 to 120 km Due to O_2 and O_3 Absorption of Solar Radiation

DARRELL F. STROBEL

Plasma Dynamics Branch
Plasma Physics Division

November 1976

NAVAL RESEARCH LABORATORY
Washington, D.C.

SECURITY CLASSIFICATION OF THIS PAGE (When Data Entered)

REPORT DOCUMENTATION PAGE		READ INSTRUCTIONS BEFORE COMPLETING FORM
1. REPORT NUMBER NRL Memorandum Report 3398	2. GOVT ACCESSION NO.	3. RECIPIENT'S CATALOG NUMBER 9 Memorandum rept.,
4. TITLE (and Subtitle) 6 PARAMETERIZATION OF THE ATMOSPHERIC HEATING RATE FROM 15 to 120 KM DUE TO O_2 AND O_3 ABSORPTION OF SOLAR RADIATION.		5. TYPE OF REPORT & PERIOD COVERED Interim report on a continuing NRL problem.
		6. PERFORMING ORG. REPORT NUMBER
7. AUTHOR(s) 10 Darrell F. Strobel		8. CONTRACT OR GRANT NUMBER(s)
9. PERFORMING ORGANIZATION NAME AND ADDRESS Naval Research Laboratory Washington, D.C. 20375		10. PROGRAM ELEMENT, PROJECT, TASK AREA & WORK UNIT NUMBERS NRL Problem A03-23 N00019-76-WR-61127
11. CONTROLLING OFFICE NAME AND ADDRESS Naval Air Systems Command Washington, D.C. 20361		12. REPORT DATE 11 November 1976
		13. NUMBER OF PAGES 42
14. MONITORING AGENCY NAME & ADDRESS(if different from Controlling Office) 12 29p.		15. SECURITY CLASS. (of this report) UNCLASSIFIED
		15a. DECLASSIFICATION/DOWNGRADING SCHEDULE

16. DISTRIBUTION STATEMENT (of this Report)

Approved for public release; distribution unlimited.

14 NRL-MR-3398

17. DISTRIBUTION STATEMENT (of the abstract entered in Block 20, if different from Report)

18. SUPPLEMENTARY NOTES

19. KEY WORDS (Continue on reverse side if necessary and identify by block number)

Stratosphere
Mesosphere
Atmospheric heating

20. ABSTRACT (Continue on reverse side if necessary and identify by block number)

The atmospheric heating rate due to O_2 (oxygen) and O_3 (ozone) absorption of solar radiation is parameterized with an accuracy of ± 5 percent in the altitude region 15-120 km. For relevant wavelengths the effects of multiple scattering and ground reflection are also included. These parameterizations are computationally fast, efficient, and suitable for use in numerical models of atmospheric circulation.

DD FORM 1 JAN 73 1473 EDITION OF 1 NOV 65 IS OBSOLETE
S/N 0102-014-6601

SECURITY CLASSIFICATION OF THIS PAGE (When Data Entered)

251950

CONTENTS

PARAMETERIZATION OF THE ATMOSPHERIC HEATING RATE FROM 15 TO 120 KM DUE TO O_2 AND O_3 ABSORPTION OF SOLAR RADIATION

INTRODUCTION

In order to numerically simulate the earth's upper atmospheric circulation, accurate and computationally efficient parameterizations of solar radiative heating are required. Of major interest is the solar radiative heating by ozone absorption in the Hartley region (2000-3000Å), Huggins bands (3000-3500Å) and the Chappius bands (4500-7500Å). Above the mesopause O_2 absorption of solar uv radiation in the Schumann-Runge bands (1750-2050Å) and Schumann-Runge continuum (1250-1750Å) must also be included.

For ozone heating rates two different parameterizations have been previously developed. Lindzen and Will (1973) assumed that the O_3 absorption cross sections are either constant or have an exponential variation over individual wavelength intervals. With these assumptions, they obtained simple analytic formulas for the O_3 heating rate. The advantage of this method is that improved solar flux and/or cross section data can easily be incorporated into the parameterization scheme. An alternate approach has been developed by Lacis and Hansen (1974) for general circulation models. They found analytic expressions for the O_3 heating rate profiles by numerical fits to exact profiles. However, to incorporate revised solar flux and/or cross section data this method requires a repetition of their fitting procedures to obtain new numerical coefficients. This approach is obviously not as flexible in some respects as the Lindzen and Will (1973) formulas. Accordingly, the latter is adopted to represent O_2 and O_3 heating rates by insolation from 15 to 120 km.

Note: Manuscript submitted October 18, 1976.

EXACT HEATING RATE CALCULATION

To develop parameterizations for any atmospheric circulation model, it is best to have "exact" or detailed calculations available to assess their accuracy. The solar fluxes and the O_2 and O_3 absorption cross sections adopted for the exact calculation are tabulated in Table 1. Since we will indicate how to incorporate improved fluxes and cross sections in the parameterizations, we do not need to justify the selected input data (e.g., the controversial solar flux values in the 1750-2050Å region).

The solar fluxes were selected from the following sources: Broadfoot (1972), Brueckner _et al_. (1976), CIAP Monograph 1, Donnelly and Pope (1973) and Smith and Gottlieb (1975). The O_2 and O_3 cross sections are based on Blake (1973), CIAP Monograph 1, Hudson (1971) and Hudson and Mahle (1972). Calculation of the O_2 and O_3 heating rates is straightforward for all wavelengths of interest with the exception of solar radiation penetration through the absorbing O_2 Schumann-Runge bands (1750-2050Å). McConnell (1974) has noted that transmission of solar radiation in each band _i_, Tr_i, can be adequately represented by

$$Tr_i = \exp\left\{-(\gamma_i N_2 + \delta_i N_2^{1/2})\right\} \quad (1)$$

where N_2 is the column density of O_2 along the solar radiation path, γ_i and δ_i are coefficients given in Table 2. The total O_2 heating rate in the Schumann-Runge bands (SRB) is

$$Q_{SRB}(O_2) = \sum_{i=1}^{19} F_i \sigma_i Tr_i [O_2] \quad (2)$$

where F_i is the solar flux integrated over each band, $[O_2]$ is the O_2 number density and the cross section (σ_i) is given by

$$\sigma_i^{-1} = \alpha_i + \beta_i N_2^{\frac{1}{2}} \tag{3}$$

with α_i and β_i tabulated in Table 2. An accuracy of within 20 percent of the experimental data of Hudson and Mahle (1972) can be achieved with these expressions and coefficients. The O_2 column density was computed using a 16 point Gaussian quadrature integration scheme.

Net heating rates (εQ) defined as the energy absorbed minus the chemical energy stored by the dissociated products were computed with efficiency factors,

$$\varepsilon_j = \left(\frac{hc}{\lambda_j} - D\right) / \frac{hc}{\lambda_j} \tag{4}$$

where D is the dissociation energy of the absorbing molecules (1.05 ev for O_3 and 5.12 ev for O_2), λ_j is the wavelength of the photon, h is Planck's constant and c is the speed of light.

PARAMETERIZATION OF THE O_3 HEATING RATE

For the Chappius bands (c) we follow Lindzen and Will (1973) and write the O_3 heating rate (Q_c) as

$$\frac{Q_c}{[O_3]} = F_c \, \sigma_c \, e^{-\sigma_c N_3} \tag{5}$$

where $[O_3]$ is the O_3 number density and N_3 its column density along the solar radiation path. We find that

$$F_c = 3.7 \times 10^5 \text{ ergs cm}^{-2}\text{sec}^{-1}$$
$$\sigma_c = 2.85 \times 10^{-21} \text{ cm}^2 \tag{6}$$

gives the best fit to exact calculations of Q_c. σ_c is 0.62 times the peak O_3 cross section at ~6000Å and F_c is 0.7 times the integrated flux over the Chappius bands. The net heating rate $\varepsilon_c Q_c$ is obtained with λ_j = 6000Å for the efficiency factor ε_c from equation (4).

A similar approximation is appropriate for the Hartley region (Ha) from 2425-2775Å. Thus

$$\frac{Q_{Ha}}{[O_3]} = F_{Ha} \, \sigma_{Ha} \, e^{-\sigma_{HA} N_3} \tag{7}$$

where

$$F_{Ha} = 5460 \text{ ergs cm}^{-2}\text{sec}^{-1}$$
$$\sigma_{Ha} = 8.8 \times 10^{-18} \text{ cm}^2 \tag{8}$$

with σ_{Ha} equal to 0.8 times the peak O_3 cross section at ~2525Å and F_{Ha} the integrated flux over the 2425-2775Å interval. The net heating rate $\varepsilon_{Ha} Q_{Ha}$ is calculated with λ_j = 2500Å in equation (4).

In the Huggins bands (Hu, defined here as the 2775-3600Å interval) we assume, as Lindzen and Will (1973), that the O_3 cross section has an exponential variation

$$\sigma = \sigma_{Hu} e^{-M\lambda} . \tag{9}$$

To obtain greater accuracy than Lindzen and Will (1973), we break the Huggins bands up into two intervals. The heating rate is

$$\frac{Q_{Hu}}{[O_3]} = \int_{\lambda_{long}}^{3600Å} I_1 \sigma e^{-\sigma N_3} d\lambda + \int_{\lambda_{short}}^{\lambda_{long}} I_2 \sigma e^{-\sigma N_3} d\lambda$$

or

$$\frac{Q_{Hu}}{[O_3]} = \frac{1}{MN_3} \Big\{ I_1 + (I_2 - I_1) \exp\left[-\sigma_{Hu} N_3 e^{-M\lambda_{long}}\right] \tag{10}$$

$$- I_2 \exp\left[-\sigma_{Hu} N_3 e^{-M\lambda_{short}}\right] \Big\}$$

where the atmosphere is optically thin at 3600Å. Numerically, an excellent fit to the exact heating rate is obtained with

I_1 = 59.2 ergs cm^{-2}sec^{-1} Å^{-1}

I_2 = 49.3 ergs cm^{-2}sec^{-1} Å^{-1}

M = 0.0127 Å^{-1}

λ_{short} = 2805 Å

$$\lambda_{long} = 3055 \text{ Å}$$

$$\sigma_{Hu} = 0.0125 \text{ cm}^2 . \qquad (11)$$

The intensities I_1 and I_2 can be related to fluxes integrated over the respective wavelength intervals. $\Delta\lambda_1 = 3600 - \lambda_{long} = 345\text{Å}$ and $\Delta\lambda_2 = \lambda_{long} - \lambda_{short} = 250\text{Å}$. Thus, $F_1 = I_1\Delta\lambda_1 = 2.04 \times 10^4$ ergs $\text{cm}^{-2}\text{sec}^{-1}$ and $F_2 = I_2\Delta\lambda_2 = 1.23 \times 10^4$ ergs $\text{cm}^{-2}\text{sec}^{-1}$. From Table 1 the integrated flux over interval 1 is 4.4×10^4 ergs $\text{cm}^{-2}\text{sec}^{-1}$ and F_1 is 0.46 times this value, while the integrated flux over the 2775-3055Å interval is 1.25×10^4 ergs $\text{cm}^{-2}\text{sec}^{-1}$ and F_2 is equal to this flux. In interval 1 the atmosphere is partially optically thin and all photons are not absorbed.

In the Herzberg continuum (2060-2425Å) both O_2 and O_3 absorb solar radiation and the principal region of heating occurs at 35-55 km. Adequate representation of this heating (Q_{Hz}) can be obtained with

$$Q_{Hz} = F_{Hz} \left\{\sigma_{Hz}(O_2)[O_2] + \sigma_{Hz}(O_3)[O_3]\right\} \exp \left[-\sigma_{Hz}(O_2)N_2 - \sigma_{Hz}(O_3)N_3\right] \qquad (12)$$

and

$$F_{Hz} = 1.5 \times 10^3 \text{ ergs cm}^{-2}\text{sec}^{-1}$$

$$\sigma_{Hz}(O_2) = 6.6 \times 10^{-24} \text{ cm}^2$$

$$\sigma_{Hz}(O_3) = 4.9 \times 10^{-18} \text{ cm}^2$$

$$\lambda_j = 2290\text{Å to calculate } \varepsilon_{Hz}$$

where F_{Hz} is 0.79 times the integrated flux in this wavelength region.

The parameterizations for the Chappius, Huggins, and Hartley bands are accurate to better than 2 percent. With the inclusion of

the Herzberg continuum parameterization the accuracy for the summed O_3 heating rates decreases to 5 percent, primarily because equation (12) underestimates the actual heating rate below 42 km. In Figures 1 and 2 the individual contributions to the total and net heating rates, respectively, are illustrated based on the above parameterizations. They are diurnally-averaged heating rates at the equator during equinox. The model atmosphere used in the computations is given in Table 3. Conversion factors for heating rates in $^{o}K\ day^{-1}$ to ergs $cm^{-3}\ sec^{-1}$ are given in Table 4.

Above 45 km O_3 absorption in the Hartley region is the dominant heat source, whereas below 28 km the Chappius band absorption is dominant. In the intermediate region the Huggins bands dominate. The secondary peak in the heating rate at ~85 km corresponds to the secondary maximum in the O_3 concentration in the model atmosphere. Thus, thermodynamically, this $[O_3]$ peak is expected to be quite important and its absolute value must be accurately known. Absorption in the Herzberg continuum makes a small contribution to the heating rate.

PARAMETERIZATION OF THE O_2 HEATING RATE

The Schumann-Runge continuum (SRC) can be split up into two main regions: 1250-1520Å where the O_2 cross section $\sim 10^{-17}$ cm^2, and 1520-1750Å where the O_2 cross section is proportional to $e^{-M\lambda}$. For the 1250-1520Å region we may approximate the heating as

$$\frac{Q_{SRC}}{[O_2]} = F_{SRC}\ \sigma_{SRC}\ e^{-\sigma_{SRC} N_2} \qquad (13)$$

with

$$F_{SRC} = 1.1 \text{ erg cm}^{-2} \text{ sec}^{-1}$$

$$\sigma_{SRC} = 1 \times 10^{-17} \text{ cm}^2$$

$$\varepsilon_{SRC} = 0.41 \text{ for net heating}$$

where F_{SRC} is the integrated flux over this wavelength region and σ_{SRC} is the average cross section. For the 1520-1750Å region we divide it into two intervals with $\sigma(O_2) \propto e^{-M\lambda}$ and obtain a total heating rate of

$$\frac{Q_{SRC}}{[O_2]} = \frac{1}{N_2}\left\{\frac{I_\ell}{M} e^{-\sigma_\ell N_2} + \frac{I_s - I_\ell}{M} e^{-\sigma_m N_2} - \frac{I_s}{M} e^{-\sigma_s N_2}\right\} \qquad (14)$$

where $\underline{\ell}$ denotes long wavelength end of spectrum, $\underline{s}$ denotes short wavelength end and σ_m denotes O_2 cross section at the junction of these intervals ($\sim$1660Å). The following values were found to give an excellent fit

$$
\begin{aligned}
\frac{I_\ell}{M} &= 3.43 \text{ ergs cm}^{-2}\text{sec}^{-1} \\
\frac{I_s}{M} &= 1.35 \text{ ergs cm}^{-2}\text{sec}^{-1} \\
\sigma_\ell &= 2.9 \times 10^{-19} \text{ cm}^2 \\
\sigma_m &= 1.54 \times 10^{-18} \text{ cm}^2 \\
\sigma_s &= 1.1 \times 10^{-17} \text{ cm}^2 \ .
\end{aligned}
\tag{15}
$$

$\frac{I_\ell}{M}$ is approximately 0.6 times the integrated solar flux in the 1660-1750Å interval, while $\frac{I_s}{M}$ is approximately 0.5 times the solar flux in the 1520-1660Å interval. The O_2 cross sections σ_ℓ, σ_m, and σ_s are approximately the values at 1750, 1660, and 1520Å, respectively. To compute the net heating rate we recommend

$$
\begin{aligned}
\frac{\varepsilon I_\ell}{M} &= 0.98 \text{ ergs cm}^{-2}\text{sec}^{-1} \\
\frac{\varepsilon I_s}{M} &= 0.43 \text{ ergs cm}^{-2}\text{sec}^{-1} \\
\sigma_\ell &= 2.9 \times 10^{-19} \text{ cm}^2 \\
\sigma_m &= 1.7 \times 10^{-18} \text{ cm}^2 \\
\sigma_s &= 1.15 \times 10^{-17} \text{ cm}^2
\end{aligned}
\tag{16}
$$

where $\varepsilon \simeq 0.3$.

The main contribution to atmospheric heating from the O_2 Schumann-Runge bands (SRB) occurs in the 60-100 km region. In view of the uncertainty in the solar flux magnitude in the Schumann-Runge bands coupled with the complexity of its transmission through the atmosphere, we demand only an accuracy of ± 20 percent in this parameterization. The following expression represents the total

heating rate in the 60-100 km region

$$\frac{Q_{SRB}}{[O_2]} = \frac{1}{aN_2 + bN_2^{1/2}} \tag{17}$$

where

$$a = 0.143 \text{ cgs units}$$

$$b = 9.64 \times 10^8 \text{ cgs units} \tag{18}$$

and if $N_2 < 10^{18}$ cm^2, then

$$\frac{Q_{SRB}}{[O_2]} = 9.03 \times 10^{-9} \text{ ergs sec}^{-1} . \tag{19}$$

For the net heating rate we obtain

$$a = 0.67 \text{ cgs units}$$

$$b = 3.44 \times 10^9 \text{ cgs units} \tag{20}$$

and if $N < 10^{18}$ cm^2, then

$$\frac{Q_{SRB}}{[O_2]} = 2.43 \times 10^{-19} \text{ ergs sec}^{-1} . \tag{21}$$

By appropriate scaling of both coefficients, heating rates for alternate solar flux values can be obtained.

The individual contributions to the O_2 heating rates from the above parameterizations are shown in Figures 1 and 2. Near 60 km the total O_2 heating rate is accurate only to $\pm$ 25 percent, but above 75 km it improves to within 5 percent. Heating in the Schumann-Runge bands is the dominant heat source between 88 and 96 km, while absorption in the SR continuum is most important above 96 km. The relative

importance of the SR bands in the 80-90 km region depends significantly on the O_3 concentration there.

The overall accuracy of the parameterized heating rates is $\pm$ 5 percent over the altitude region 15-120 km. Below approximately 80 km the $O(^3P)$ formed by O_3 and O_2 dissociation recombines quickly, and the actual heating rate of the atmosphere is the total photon energy absorbed. Above 80 km the $O(^3P)$ produced by O_3 and O_2 dissociation may be transported significantly in the vertical direction before recombining, and the actual heating rate is the net heating rate (εQ) plus the chemical energy released by locally recombining $O(^3P)$. To a good first approximation we can estimate the actual heating rate by summing the total O_3 heating rate and the net O_2 heating rate. In Figure 3 this estimated actual heating rate is illustrated for solstitial conditions. Only the latitudinal variation of solar radiation was included; the model atmosphere was invariant with latitude. Our heating rate agrees well with the results of Park and London (1974) when the comparison is made at the same density levels.

PARAMETERIZATION OF DIFFUSE SCATTERED SOLAR RADIATION

Solar radiation longward of 3000Å is not strongly absorbed in the earth's atmosphere and can undergo multiple scattering in the atmosphere by molecules and particles. Fortunately, in atmospheric heating calculations the major scattering effects are in the Chappius bands region of the solar spectrum (Lacis and Hansen, 1974). Their results strongly suggest that the diffuse solar radiation can be modeled by a pure O_3 absorption region on top of a reflecting layer with an effective albedo ($\overline{\omega}_o$) that depends on the ground reflectivity (R_g) and lower atmosphere albedo (R_a) as follows:

$$\overline{\omega}_o = R_a + [1 - R_a] \frac{0.856\ R_g}{1 - 0.144\ R_g} \quad . \tag{22}$$

Let the vertical optical depth due to O_3 absorption be

$$\tau^* = \int_0^\infty \sigma n dz \tag{23}$$

where n is the O_3 number density, σ is its cross section, z is height, and $d\tau = -\sigma n dz$. With θ as the solar zenith angle and s as the distance along the solar radiation path (increasing in positive value with decreasing z), we define $\mu = \cos\theta$ and $\mu ds = -dz$. The intensity (I) of the solar radiation is separated into upward (I^+) and downward (I^-) components. The associated flux is

$$F = \int_{-1}^{1} I\ \mu d\mu = \int_0^1 I^+\ \mu d\mu + \int_{-1}^{0} I^-\ \mu d\mu \tag{24}$$

and the corresponding heating rate is

$$Q = -\nabla \cdot F = -\int_{-1}^{1} \frac{dI}{dz} \mu d\mu \tag{25}$$

for a plane parallel atmosphere. For visible sunlight in the purely absorbing atmosphere the equation of transfer is simply

$$\mu \frac{dI}{d\tau} = I \tag{26}$$

since atmospheric thermal emission is negligible. Equation (26) has the solution

$$I = I_0 e^{\frac{\tau}{\mu}} . \tag{27}$$

For the downward intensity component the boundary condition is applied at the top of the atmosphere and is

$$I^-(\tau = 0,\mu) = F_\Theta \delta(\mu + \mu_0) \tag{28}$$

where F_Θ is the downward directed solar flux with direction μ_0. Thus

$$I^-(\tau,\mu) = F_\Theta \delta(\mu + \mu_0) e^{\frac{\tau}{\mu}} , \mu < 0 . \tag{29}$$

For the upward intensity component the boundary condition is applied at the reflecting surface ($\tau = \tau^*$) and is a Lambert surface with albedo ($\bar{\omega}_o$),

$$I^+(\tau^*,\mu) \text{ is isotropic}$$

$$F^+ = \bar{\omega}_o F^- \text{ at } \tau = \tau^* . \tag{30}$$

Then at τ^*

$$F^+ = \int_0^1 I^+(\tau^*,\mu)\,\mu d\mu = \tfrac{1}{2} I^+(\tau^*,\mu) = \tilde{\omega}_0 \int_{-1}^0 I^-(\tau^*,\mu)\,\mu d\mu$$

or with equation (24)

$$I^+(\tau^*,\mu) = 2\tilde{\omega}_o \mu_o F_\Theta e^{-\frac{\tau^*}{\mu_0}} \tag{31}$$

and

$$I^+(\tau,\mu) = 2\tilde{\omega}_0 \mu_0 F_\Theta e^{-\frac{\tau^*}{\mu_0}} e^{-\frac{(\tau^*-\tau)}{\mu}}, \quad \mu > 0 \,. \tag{32}$$

Since $d\tau = -\sigma n dz$, equation (25) becomes upon substitution of equation (26)

$$Q = \sigma n \int_{-1}^{1} I d\mu$$

and integration over all angles with the upward (32) and downward (29) components of intensity gives

$$Q = F_\Theta e^{-\frac{\tau}{\mu_0}} \sigma n + 2\tilde{\omega}_0 \mu_0 F_\Theta e^{-\frac{\tau^*}{\mu_0}} E_2(\tau^*-\tau)\,\sigma n \tag{33}$$

where the exponential integral E_2

$$E_2(x) = \int_0^1 d\mu\, e^{-\frac{x}{\mu}}$$

represents the transmission of the reflected light off the surface. This second term in equation (33) is thus the heating due to diffuse

reflected and scattered solar radiation, whereas the first term in equation (33) represents direct solar radiation heating.

Lacis and Hansen (1974) recommend a simple approximation for the transmission function E_2. It is

$$E_2(\tau^*-\tau) \simeq e^{-(\tau^*-\tau)M}$$

where M is the magnification factor for the vertical optical depth and has an effective value of 1.9 for diffuse radiation.

Comparisons of their detailed calculations with the results obtained from the following expression

$$Q = F_{\Theta}\sigma n \left\{ e^{-\frac{\tau}{\mu_0}} + 2\tilde{\omega}_0\mu_0 e^{-\frac{\tau^*}{\mu_0}} e^{-1.9(\tau^*-\tau)} \right\} \tag{34}$$

show good agreement for diffuse radiative heating (within 10 percent). If the effective albedo is $\tilde{\omega}_0 = 0.25$, a reasonable global average, then the O_3 heating rate from Chappius bands absorption is increased by 30 percent throughout the ozone layer due to diffuse solar radiation. This description of diffuse radiation should also prove adequate for the 3000-4000Å solar uv radiation.

SUMMARY

The atmospheric heating rates due to O_2 and O_3 absorption of solar radiation have been successfully parameterized with an accuracy of $\pm$ 5 percent from 15 to 120 km. In addition, the diffuse solar radiation produced by multiple scattering and ground reflection has been adequately described with a simple radiative transfer model of a purely absorbing layer on top of a reflecting layer. These parameterizations are suitable for use in complex numerical models of atmospheric circulation.

ACKNOWLEDGMENTS

I would like to thank J. C. McConnell for communicating the Schumann-Runge Band Coefficients in Table 2 used to generate the "exact" heating rate calculation. This research was supported by the Naval Air Systems Command.

REFERENCES

Blake, D. W., Simplified photochemical models and their applications in the stratosphere and mesosphere, Ph.D. Thesis, University of Chicago, 1973.

Broadfoot, A. L., The solar spectrum 2100-3200Å, Astrophys. J., 173, 681, 1972.

Brueckner, G. E., J. D. F. Bartoe, O. K. Moe and M. E. VanHoosier, Absolute solar ultraviolet intensities and their variations with solar activity, Astrophys. J., in press, 1976.

CIAP Monograph 1: The natural stratosphere of 1974, Dept. of Transportation, DOT-TST-75-51, Washington, D.C., 1975.

Donnelly, R. F. and J. H. Pope, The 1-3000Å solar flux for a moderate level of solar activity for use in modeling the ionosphere and upper atmosphere, Tech. Rep. ERL 276-SEL25, NOAA, Boulder, CO, 44 pp., 1973.

Hudson, R. D., Critical review of ultraviolet photo absorption cross sections for molecules of astrophysical and aeronomic interest, Rev. Geophys. Space Phys., 9, 305, 1971.

Hudson, R. D. and S. H. Mahle, Photo dissociation of moelcular oxygen in the mesosphere and lower thermosphere, J. Geophys. Res., 77, 2902, 1972.

Lacis, A. A. and J. E. Hansen, A parameterization for the absorption of solar radiation in the earth's atmosphere, J. Atmos. Sci., 31, 118, 1974.

Lindzen, R. S. and D. I. Will, An analytic formula for heating due to ozone absorption, J. Atmos. Sci., 30, 513, 1973.

McConnell, J. C., Private communication, 1974.

Smith, E. V. P. and D. M. Gottlieb, Solar flux and its variations in possible relationships between solar activity and meteorological phenomena, NASA SP-366, Washington, D.C., 1975.

Table 1: Solar Fluxes and Absorption Cross Sections*

λ(Å)	Flux (ergs cm^{-2} sec^{-1})	$\sigma(O_2)(cm^2)$	$\sigma(O_3)(cm^2)$
7500	1.27(4)		3.5(-22)
7400	1.30(4)		3.8(-22)
7300	1.34(4)		4.2(-22)
7200	1.37(4)		5.4(-22)
7100	1.40(4)		6.5(-22)
7000	1.43(4)		8.2(-22)
6900	1.47(4)		1.0(-21)
6800	1.50(4)		1.3(-21)
6700	1.54(4)		1.6(-21)
6600	1.54(4)		2.0(-21)
6500	1.56(4)		2.4(-21)
6400	1.62(4)		2.9(-21)
6300	1.65(4)		3.4(-21)
6200	1.68(4)		3.9(-21)
6100	1.72(4)		4.5(-21)
6000	1.75(4)		4.6(-21)
5900	1.78(4)		4.0(-21)
5800	1.82(4)		4.3(-21)
5700	1.83(4)		4.3(-21)
5600	1.83(4)		3.5(-21)
5500	1.85(4)		3.1(-21)
5400	1.89(4)		2.7(-21)
5300	1.89(4)		2.3(-21)
5200	1.85(4)		1.7(-21)
5100	1.87(4)		1.5(-21)
5000	1.93(4)		9.4(-22)
4900	1.92(4)		6.7(-22)
4800	1.94(4)		5.7(-22)
4700	1.99(4)		2.7(-22)
4600	2.00(4)		2.4(-22)
4500	1.97(4)		1.2(-22)
3550	9.5(3)		3.5(-22)
3450	8.9(3)		1.0(-21)
3350	9.0(3)		4.2(-21)
3250	7.8(3)		1.5(-20)
3150	6.4(3)		6.2(-20)
3075	2.6(3)		1.5(-19)
3000	3.9(3)		3.5(-19)
2925	5.2(3)		1.2(-18)
2825	2.4(3)		3.3(-18)
2725	2.4(3)		6.8(-18)
2625	1.9(3)		1.0(-17)
2525	8.1(2)		1.1(-17)
2450	3.5(2)		9.8(-18)
2400	2.9(2)	5.0(-25)	8.2(-18)
2350	2.9(2)	1.4(-24)	6.4(-18)
2300	3.1(2)	3.3(-24)	4.5(-18)
2250	3.4(2)	5.3(-24)	3.0(-18)

Table 1: Solar Fluxes and Absorption Cross Sections* - Cont.

λ(Å)	Flux (ergs cm^{-2} sec^{-1})	$\sigma(O_2)(cm^2)$	$\sigma(O_3)(cm^2)$
2200	2.9(2)	7.6(-24)	1.8(-18)
2150	2.4(2)	9.6(-24)	1.0(-18)
2100	1.5(2)	1.1(-23)	5.5(-19)
2060	2.0(1)	1.3(-23)	3.8(-19)
2025	1.7(1)	See Table 2	3.3(-19)
2000	1.4(1)	"	3.1(-19)
1985	7.0(0)	"	3.3(-19)
1972	5.8(0)	"	3.6(-19)
1947	1.0(1)	"	4.1(-19)
1924	7.0(0)	"	4.5(-19)
1902	6.5(0)	"	5.2(-19)
1882	5.2(0)	"	5.9(-19)
1863	4.2(0)	"	6.5(-19)
1846	2.8(0)	"	6.8(-19)
1830	2.7(0)	"	7.0(-19)
1816	2.5(0)	"	7.3(-19)
1804	1.8(0)	"	7.5(-19)
1793	1.3(0)	"	7.7(-19)
1783	1.2(0)	"	7.9(-19)
1775	8.1(-1)	"	8.1(-19)
1769	6.7(-1)	"	8.2(-19)
1763	1.3(0)	"	8.2(-19)
1750	1.0(0)	"	8.3(-19)
1740	1.7(0)	3.7(-19)	
1720	1.5(0)	5.9(-19)	
1700	1.3(0)	8.5(-19)	
1680	8.7(-1)	1.2(-18)	
1660	7.7(-1)	1.8(-18)	
1640	5.6(-1)	2.5(-18)	
1620	4.0(-1)	3.4(-18)	
1600	3.2(-1)	4.7(-18)	
1580	2.9(-1)	6.0(-18)	
1560	3.4(-1)	7.3(-18)	
1540	3.3(-1)	8.5(-18)	
1520	2.0(-1)	1.0(-17)	
1500	1.5(-1)	1.1(-17)	
1480	1.3(-1)	1.2(-17)	
1460	1.1(-1)	1.3(-17)	
1440	8.3(-2)	1.5(-17)	
1420	7.0(-2)	1.5(-17)	
1400	1.3(-1)	1.4(-17)	
1380	4.8(-2)	1.3(-17)	
1360	6.3(-2)	8.0(-18)	
1340	1.2(-1)	2.3(-18)	
1320	4.3(-2)	1.4(-18)	
1300	7.6(-2)	5.0(-19)	
1280	6.9(-3)	2.8(-19)	
1260	1.6(-2)	4.3(-19)	

*The solar fluxes are integrated over wavelength intervals whose center value is given. Note that the values in parentheses are the powers of 10 by which the primary tabular entry is to be multipled.

Table 2: Schumann-Runge Band Coefficients (cgs units)[1].

Band	Wavelength (Å)	α_i	β_i	γ_i	δ_i
1	2025.0	8.2595(22)	6.9850(8)	1.1983(-23)	6.4880(-14)
2	2000.0	8.0106(22)	-3.5546(9)	1.2662(-23)	9.6723(-14)
3	1985.0	7.3112(22)	2.2040(9)	1.3033(-23)	3.0529(-13)
4	1971.8	1.8757(22)	1.0081(11)	1.2899(-23)	1.7876(-12)
5	1947.0	1.4252(22)	1.0586(11)	1.2204(-23)	2.6838(-12)
6	1924.0	1.2321(21)	2.5293(11)	1.4519(-23)	5.4926(-12)
7	1902.4	4.6314(20)	1.7798(11)	1.8859(-23)	8.3986(-12)
8	1882.2	1.4269(20)	1.3011(11)	1.5313(-23)	1.2232(-11)
9	1863.4	6.8431(19)	7.8005(10)	4.9293(-23)	1.9898(-11)
10	1846.2	5.9996(19)	4.6831(10)	7.7757(-23)	3.1147(-11)
11	1830.6	1.9521(19)	3.9664(10)	1.0391(-22)	3.5539(-11)
12	1816.4	7.2957(17)	3.1870(10)	2.1977(-22)	5.0541(-11)
13	1803.6	9.0621(18)	1.5782(10)	4.6920(-22)	9.0615(-11)
14	1792.6	1.2199(18)	2.4265(10)	1.1067(-21)	6.7403(-11)
15	1782.6	4.0394(18)	2.4928(10)	2.1219(-21)	6.1440(-11)
16	1774.6	8.2969(18)	1.1984(10)	3.0367(-21)	1.0362(-10)
17	1768.6	5.5205(18)	5.2439(9)	8.7466(-21)	1.8609(-10)
18	1763.2	5.0849(18)	2.5956(9)	2.1935(-20)	2.4514(-10)
19	1750.0	3.3967(18)	1.4959(9)	5.2699(-20)	3.1771(-10)

[1]These coefficients were supplied by McConnell (1974).

Table 3: Model Atmosphere

Z(km)	T(°k)	[O](cm^{-3})	[O_2](cm^{-3})	[N_2](cm^{-3}	[O_3](cm^{-3})
15	216.6	3(6)	8.586(17)	3.191(18)	2(12)
20	216.6	1(7)	3.920(17)	1.457(18)	3.1(12)
25	221.7	5(7)	1.720(17)	6.391(17)	4.5(12)
30	230.7	2(8)	7.823(16)	2.908(17)	3.1(12)
35	241.5	3.5(8)	3.651(16)	1.357(17)	1.6(12)
40	255.3	1.5(9)	1.752(16)	6.513(16)	6.7(11)
45	267.7	3(9)	8.794(15)	3.269(16)	2.1(11)
50	271.6	9(9)	4.660(15)	1.732(16)	7(10)
55	263.9	2(10)	2.565(15)	9.535(15)	2.2(10)
60	249.3	2.5(10)	1.414(15)	5.255(15)	7(9)
65	232.7	2.3(10)	7.564(14)	2.812(15)	2.2(9)
70	216.2	2(10)	3.863(14)	1.436(15)	7(8)
75	205.0	4(10)	1.824(14)	6.792(14)	2(8)
80	195.0	6.2(10)	8.204(13)	3.104(14)	3.1(8)
85	185.1	1.4(11)	3.548(13)	1.365(14)	1.2(8)
90	183.8	1.66(11)	1.422(13)	5.585(13)	2.7(7)
95	190.3	1.91(11)	5.483(12)	2.218(13)	4.6(6)
100	203.5	4.150(11)	1.991(12)	8.710(12)	1.3(6)
105	228.0	4.436(11)	6.653(11)	3.597(12)	1.5(5)
110	265.5	3.228(11)	2.500(11)	1.585(12)	1.4(4)
115	317.1	2.148(11)	1.086(11)	7.447(11)	1.2(3)
120	380.6	1.422(11)	5.420(10)	3.793(11)	1.5(2)

Table 4: Conversion Factors for $^{o}K\ day^{-1}$ to $ergs\ cm^{-3}\ sec^{-1}$

Z(km)		Z(km)	
15	2.26(-2)	70	1.02(-5)
20	1.03(-2)	75	4.80(-6)
25	4.52(-3)	80	2.19(-6)
30	2.06(-3)	85	9.59(-7)
35	9.60(-4)	90	3.90(-7)
40	4.60(-4)	95	1.54(-7)
45	2.31(-4)	100	6.01(-8)
50	1.23(-4)	105	2.43(-8)
55	6.75(-5)	110	1.06(-8)
60	3.73(-5)	115	5.07(-9)
65	1.99(-5)	120	2.63(-9)

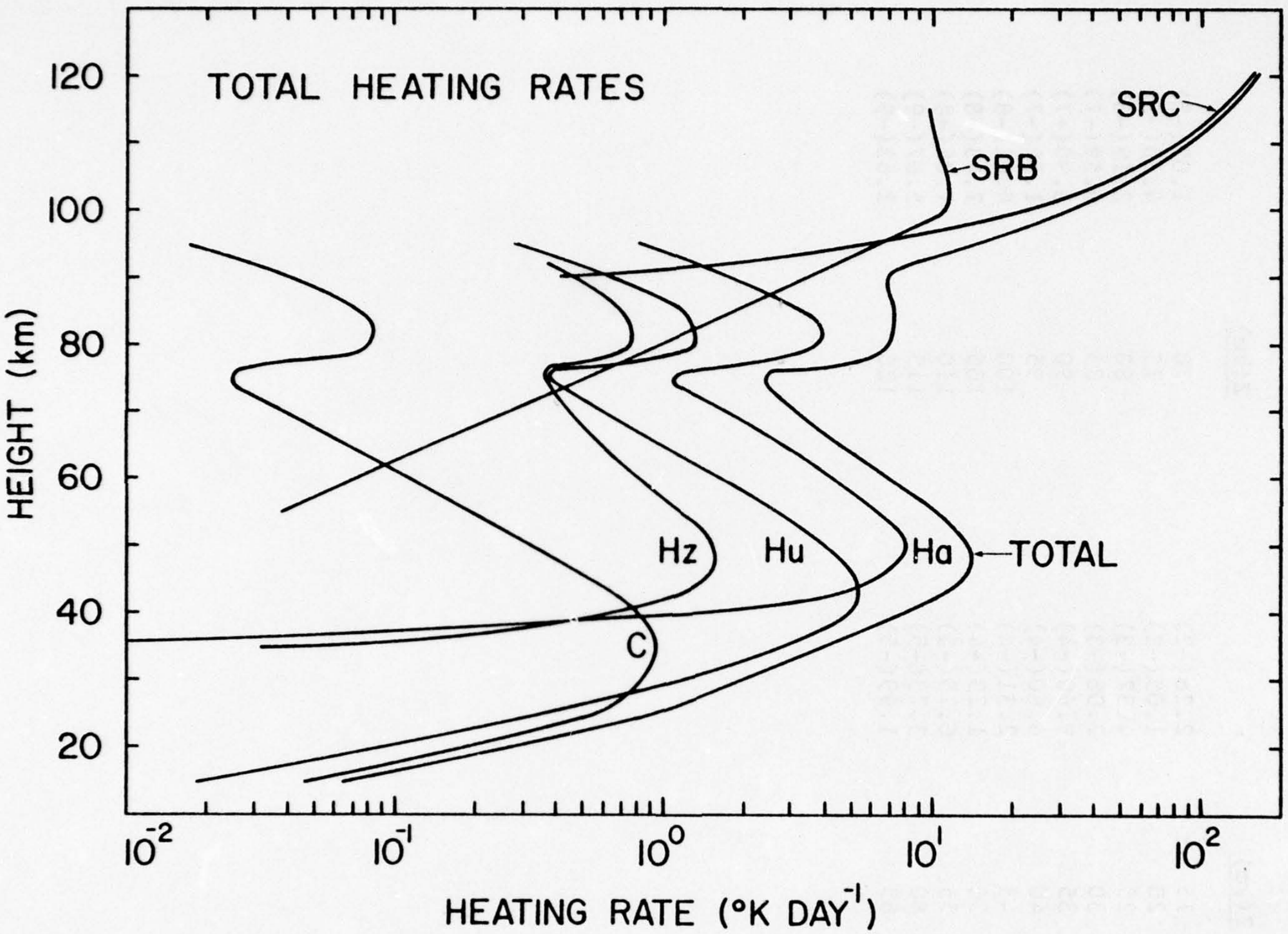

Fig. 1 — Diurnally-averaged total heating rates at the equator as a function of altitude in the Chappius (C), Huggins (Hu), Hartley (Ha), Herzberg (Hz), Schumann-Runge Bands (SRB), and Continuum (SRC) wavelength regions of the solar spectrum. Solar declination angle = 0°, equinox.

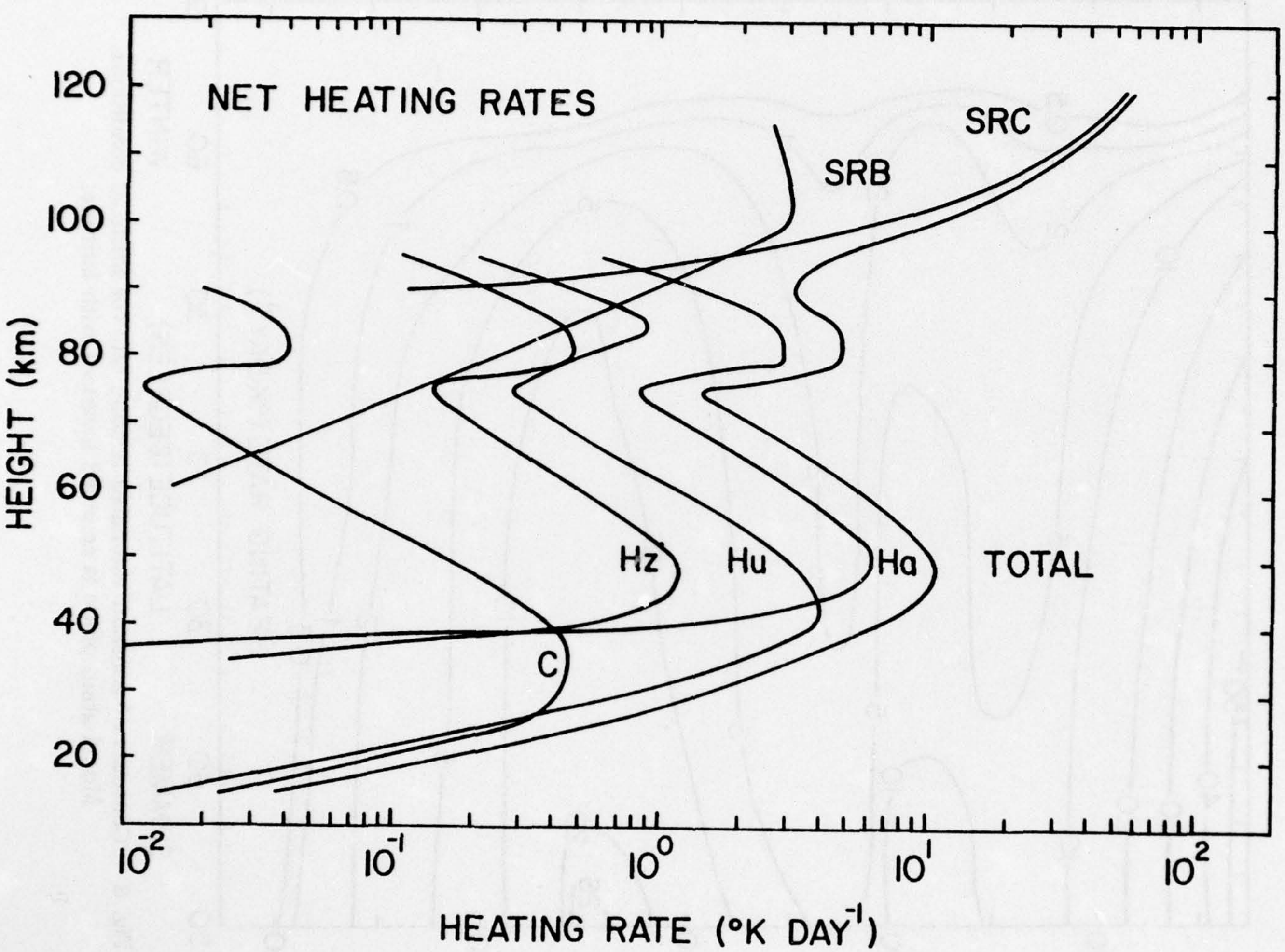

Fig. 2 — Same as Fig. 1, but for net heating rates

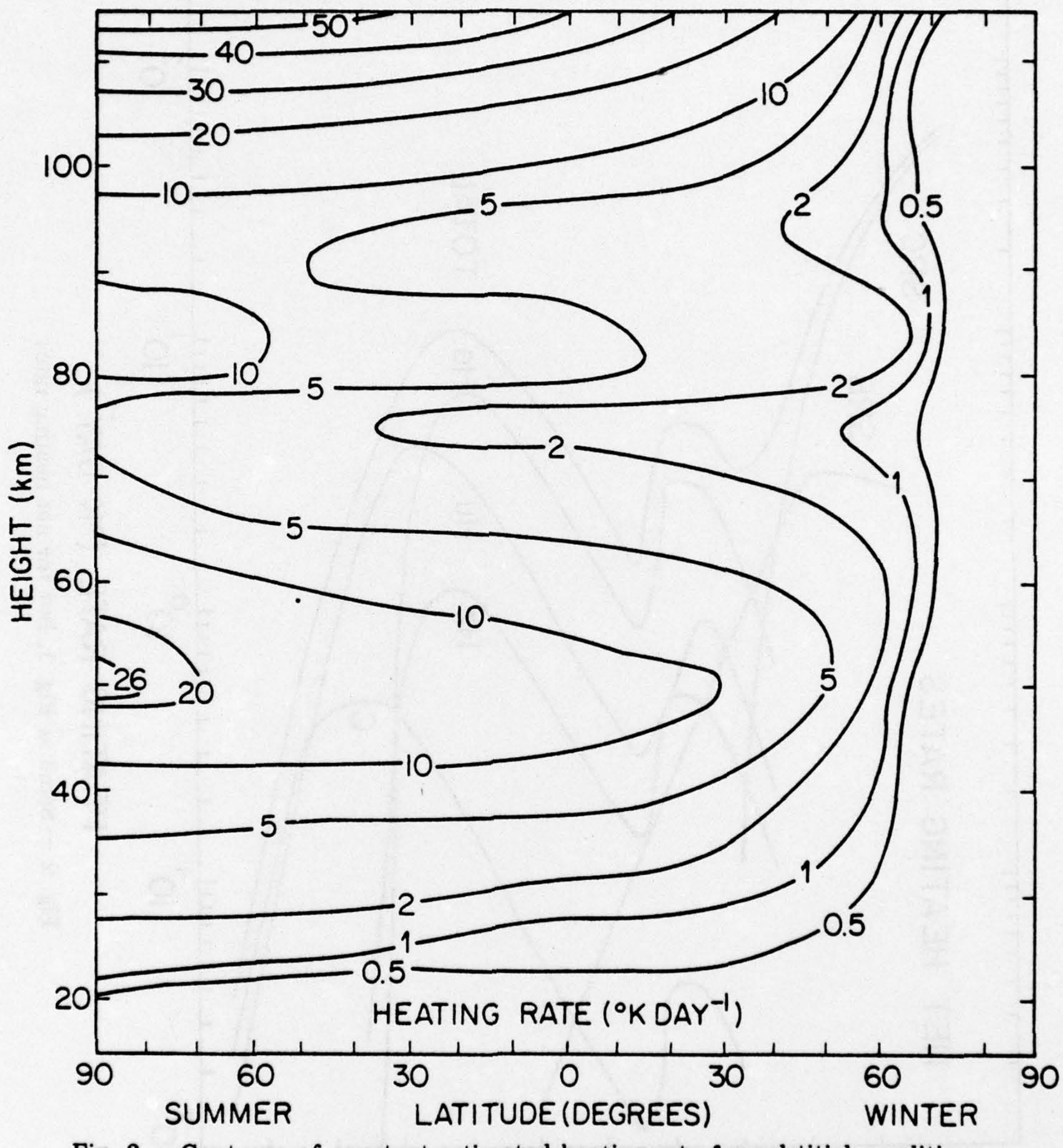

Fig. 3 — Contours of constant estimated heating rate for solstitial conditions. Model atmosphere is assumed invariant with latitude.

DISTRIBUTION LIST

DIRECTOR
Defense Advanced Rsch Proj Agency
Architect Building
1400 Wilson Blvd.
Arlington, Va. 22209
ATTN: Strategic Tech Office
ATTN: LTC. W. A. Whitaker
ATTN: STO CAPT. J. Justice

Defense Communication Engineer Center
1860 Wiehle Avenue
Reston, Va. 22090
ATTN: CODE R820 R. L. Crawford
ATTN: CODE R410 W. D. Dehart

DIRECTOR
Defense Communications Agency
Washington, D. C. 20305
ATTN: CODE 960
ATTN: CODE 480

Defense Documentation Center
Cameron Station
Alexandria, Va. 22314 — 12 copies
ATTN: TC

DIRECTOR
Defense Intelligence Agency
Washington, D. C. 20301
ATTN: W. Wittig DC - 7D
ATTN: DT - 1B

DIRECTOR
Defense Nuclear Agency
Washington, D. C. 20305
ATTN: STSI Archives
ATTN: STVL
ATTN: STTL Tech Library — 2 copies
ATTN: DDST
ATTN: RAAE
ATTN: RAAE Charles A. Blank
ATTN: Warren W. Berning
ATTN: RAAE Harold C. Fitz, Jr.
ATTN: RAAE MAJ. John Clark

DIR OF DEFENSE RSCH & ENGINEERING
Washington, D. C. 20301
ATTN: DD/S&SS John B. Walsh
ATTN: AOD/EPS LTC W. A. WHITAKER
ATTN: AD/S&AS Daniel Brockway

COMMANDER
Field Command
Defense Nuclear Agency
Kirtland AFB, NM 87115
ATTN: FCPR

Interservice Nuclear Weapons School
Kirtland AFB, NM 87115
ATTN: Document Control

DIRECTOR
Joint Strat TGT Planning Staff Jcs
Offutt AFB
Omaha, NB 68113
ATTN: JLTW-2
ATTN: JPST G. D. Burton
ATTN: JPST MAJ. J. S. Green

CHIEF
Livermore Division Fld Command DNA
Lawrence Livermore Laboratory
P. O. Box 808
Livermore, CA 94550
ATTN: FCPRL

COMMANDER
National Military Comd Sys Support Ctr
Pentagon
Washington, D. C. 20301
ATTN: B211
ATTN: DP DIRECTOR FOR CSPO

DIRECTOR
National Security Agency
Ft. George G. Meade, Md. 20755
ATTN: W14 Pat Clark
ATTN: Frank Leonard

OJCS/J-3
The Pentagon
Washington, D. C. 20301
ATTN: J-3 OPS ANAL BR. COL. Underhill

OJCS/J-6
The Pentagon
Washington, D. C. 20301
ATTN: J-6

DIRECTOR
Telecommunications & Comd & Con Sys
Washington, D. C. 20301
ATTN: ASST DIR Info & Space Sys
ATTN: DEP ASST. SEC Sys

Weapons Systems Evaluation Group
400 Army-Navy Drive
Arlington, Va. 22202
ATTN: DOCUMENT CONTROL

COMMANDER
Harry Diamond Laboratories
2800 Powder Mill Road
Adelphi, Md. 20783
ATTN: AMXDO-NP

COMMANDER
TRASANA
White Sands Missile Range, NM 88002
ATTN: EAB

DIRECTOR
U. S. Army Ballistic Research Labs
Aberdeen Proving Ground, Md. 21003
ATTN: AM-CA Franklin E. Niles

U. S. Army Communications CMD
C-B Services Division
Pentagon Rm. 2D513
Washington, D. C. 20310

COMMANDER
U. S. Army Electronics Command
Fort Mommouth, N. J. 07703
ATTN: AMSEL-TL-ENV Hans A. Bomke

COMMANDER
U. S. Army Material Command
5001 Eisenhower Avenue
Alexandria, Va. 22333
ATTN: AMCRD-WN-RE John F. Corrigan

COMMANDER
U. S. Army Material Command
Foreign and Scientific Tech Center
220 7th St. N. E.
Charlottesville, Va. 22901
    ATTN: P. A. Crowley
    ATTN: R. Jones

COMMANDER
U. S. Army Missile Command
Redstone Arsenal
Huntsville, Al. 35809
    ATTN: AMSMI-YTT W. G. Preussel, Jr.

COMMANDER
U. S. Army Nuclear Agency
Fort Bliss, Tx. 79916
    ATTN: USANUA-W. J. Berbert

CHIEF of Naval Research
Department of the Navy
Arlington, Ba. 22217
    ATTN: CODE 464 Jacob L. Warner
    ATTN: CODE 464 Thomas P. Quinn

COMMANDER
Naval Air Systems Command
Headquarters
Washington, D. C. 21360
    ATTN: AIR 5381

COMMANDER
Naval Electronics Systems Command
Naval Electronic System CMD HQS
Washington, D. C. 20360
    ATTN: NAVALEX 034 T. Barry Hughes
    ATTN: PME 106-1 Satellite Comm Project Off
    ATTN: John E. Doncarlos
    ATTN: PME 117

COMMANDER
Naval Electronics Laboratory Center
San Diego, CA 92152
    ATTN: William F. Moler
    ATTN: CODE 2200 Verne E. Hildebrand
    ATTN: R. Eastman

COMMANDING OFFICER
Naval Intelligence Support CTR
1301 Suitland Road, Bldg. 5
Washington, D. C. 20390
ATTN: Mr. Dubbin Stic 12

DIRECTOR
Naval Research Laboratory
Washington, D. C. 20375
ATTN: HDQ COMM DIR Bruce Wald
ATTN: CODE 5460 Radio Propagation BR
ATTN: CODE 7701 Jack D. Brown
ATTN: CODE 7700 Division Superintendent 25 copies

ATTN: CODE 7750 Branch Head 150 copies

COMMANDING OFFICER
Naval Space Surveillance System
Dahlgren, Va. 22448

COMMANDER
Naval Surface Weapons Center
White Oak, Silver Spring, Md. 20910
ATTN: CODE 1224 Navy Nuc Prgms Off

DIRECTOR
Strategic Systems Project Office
Navy Department
Washington, D. C. 20376
ATTN: NSP-2141

COMMANDER
ADC/AD
ENT AFB, Co., 80912
ATTN: ADDA

Headquarters
U. S. Army Elect Warfare Lab (ECOM)
White Sands Missile Range, NM 88002
ATTN: E. Butterfield

AF Cambridge Rsch Labs, AFSC
L. G. Hanscom Field
Bedford, Ma 01730
ATTN: LKB Kenneth S. W. Champion
ATTN: OPR James C. Ulwick
ATTN: OP John S. Garing
ATTN: OPR Alva T. Stair

AF Weapons Laboratory, AFSC
Kirtland AFB, NM 87117
ATTN: John M. Kamm SAS
ATTN: SUL
ATTN: DYT CAPT. David W. Goetz
ATTN: DYT MAJ. Don Mitchell

AFTAC
Patrick AFB, Fl. 32925
ATTN: TF MAJ. E. Hines
ATTN: TF/CAPT. Wiley
ATTN: TN

Air Force Avionics Laboratory, AFSC
Wright-Patterson AFB, Oh. 45433
ATTN: AFAL AVWE Wade T. Hunt

Assistant Chief of Staff
Studies and Analysis
Headquarters, U. S. Air Force
Washington, D. C. 20330
ATTN: LTC. A. D. Dayton

Headquarters
Electronics Systems Division (AFSC)
L. G. Hanscom Field
Bedford, Ma. 01730
ATTN: XRE LT. Michaels
ATTN: LTC J. Morin CDEF XRC
ATTN: YSEV LTC. David C. Sparks

COMMANDER
Foreign Technology Division, AFSC
Wright-Patterson AFB, Oh. 45433
ATTN: TD-BTA LIBRARY

HQ USAF/RD
Washington, D. C. 20330
ATTN: RDQ

COMMANDER
Rome Air Development Center, AFSC
Griffith AFB, N. Y. 13440
ATTN: EMTLD Doc Library

COMMANDER IN CHIEF
Strategic Air Command
Offutt AFB, NB 68113
ATTN: XPFS MAJ. Brian G. Stephan

544IES
Offutt AFB, NB 68113
ATTN: RDPO LT. Alan B. Merrill

Los Alamos Scientific Laboratory
P. O. Box 1663
Los Alamos, NM 87544
ATTN: DOC CON for R. F. Taschek
ATTN: DOC CON for Milton Peek

Sandia Laboratories
P. O. Box 5800
Albuquerque, NM 87115
ATTN: DOC CON for A. Dean Thronbrough
ATTN: DOC CON for W. D. Brown
ATTN: DOC CON for D. A. Dahlgren, ORG 1722

University of California
Lawrence Livermore Laboratory
P. O. Box 808
Livermore, CA 94550
ATTN: Tech Info Dept L-3

Department of Commerce
National Oceanic & Atmospheric Admin.
Environmental Research Laboratories
Boulder, CO 80302
ATTN: Joseph H. Pope
ATTN: C. L. Rufenach

Department of Commerce
Office for Telecommunications
Institute for Telecom Science
Boulder, CO 80302
ATTN: Glenn Falcon
ATTN: G. Reed
ATTN: L. A. Berry

Department of Transportation
Transportation Rsch. System Center
Kendall Square
Cambridge, MA 02142
ATTN: TER G) Harowles

NASA
Goddard Space Flight Center
Greenbelt, Md 20771
ATTN: CODE 750 T. Golden

NASA
600 Independence Ave., S. W.
Washington, D. C. 20346
ATTN: M. Dubin
ATTN: J. Holtz

Aerodyne Research, Inc.
Tech/Ops Building
20 South Avenue
Burlington, MA 01803
ATTN: M. Camac
ATTN: F. Bien

Aerospace Corporation
P. O. Box 92957
Los Angeles, CA 90009
ATTN: T. M. Salmi
ATTN: S. P. Bower
ATTN: V. Josephson
ATTN: SMFA for PWW
ATTN: R. Grove
ATTN: R. D. Rawcliffe
ATTN: T. Taylor
ATTN: Harris Mayer
ATTN: D. C. Cartwright

Analytical Systems Corporation
25 Ray Avenue
Burlington, MA 01803
ATTN: Radio Sciences

Avco-Everett Research Laboratory, Inc.
2385 Revere Beach Parkway
Everett, MA 02149
ATTN: Richard M. Patrick

Boeing Company, The
P. O. Box 3707
Seattle, WA 98124
ATTN: D. Murray
ATTN: Glen Keister

Brown Engineering Company, Inc.
Cummings Research Park
Huntsville, AL 35807
ATTN: David Lambert MS 18

California at San Diego, Univ. of
Building 500 Mather Campus
3172 Miramar Road
La Jolla, CA 92037
ATTN: Henry G. Booker

Calspan
P. O. Box 235
Buffalo, N. Y. 14221
ATTN: Romeo A. Deliberis

Computer Sciences Corporation
P. O. Box 530
6565 Arlington Blvd.
Falls Church, VA 22046
ATTN: H. Blank
ATTN: Barbara F. Adams

Comsat Laboratories
P. O. Box 115
Clarksburg, Md. 20734
ATTN: R. R. Taur

Cornell University
Department of Electrical Engineering
Ithaca, N. Y. 14850
ATTN: D. T. Farley, Jr.

ESL, Inc.
495 Java Drive
Sunnyvale, CA 93102
ATTN: J. Roberts
ATTN: V. L. Mower
ATTN: James Marshall
ATTN: R. K. Stevens

General Electric Company
Tempo-Center for Advanced Studies
816 State Street
Santa Barbara, CA 93102
ATTN: Don Chandler
ATTN: DASIAC
ATTN: DASIAC Art Feryok
ATTN: Warren S. Knapp

General Electric Company
P. O. Box 1122
Syracuse, N. Y. 13201
ATTN: F. A. Reibert

General Research Corporation
P. O. Box 3587
Santa Barbara, CA 93105
ATTN: John Ise, Jr.

Geophysical Institute
University of Alaska
Fairbanks, AK 99701
ATTN: Technical Library
ATTN: Neil Brown
ATTN: T. N. Davis

GTE Sylvania, Inc.
189 B Street
Needham Heights, MA 02194
ATTN: Marshall Cross

HRB-SINGER, Inc.
Science Park, Science Park Road
P. O. Box 60
State College, PA 16801
ATTN: Larry Feathers

Honeywell Incorporated
Radiation Center
2 Forbes Road
Lexington, MA 02173
ATTN: W. Williamson

Illinois, University of
Department of Electrical Engineering
Urbana, IL 61801
ATTN: K. C. Yeh

Institute for Defense Analyses
400 Army-Navy Drive
Arlington, VA 22202
ATTN: Ernest Bauer
ATTN: Hans Wolfhard
ATTN: J. M. Aein
ATTN: Joel Bengston

Intl Tel & Telegraph Corporation
500 Washington Avenue
Nutley, N. J. 07110
ATTN: Technical Library

ITT Electro-Physics Laboratories, Inc.
9140 Old Annapolis Road
Columbus, Md. 21043
ATTN: John M. Kelso

Johns Hopkins University
Applied Physics Laboratory
8621 Georgia Avenue
Silver Spring, MD 20910
ATTN: Document Librarian

Lockheed Missiles & Space Co., Inc.
P. O. Box 504
Sunnyvale, CA 94088
ATTN: Dept. 60-12

Lockheed Missiles and Space Company
3251 Hanover Street
Palo Alto, CA 94304
ATTN: Billy M. McCormac, Dept 52-14
ATTN: Martin Walt, Dept 52-10
ATTN: Richard G. Johnson, Dept 52-12
ATTN: J. B. Reagan, Dept 52-12
ATTN: John Kumer
ATTN: Robert D. Sears, Dept 52-14

MIT Lincoln Laboratory
P. O. Box 73
Lexington, MA 02173
ATTN: Mr. Walden, X113
ATTN: D. Clark
ATTN: James H. Pannell, L-246
ATTN: Lib A-082 for David M. Towle

Martin Marietta Corporation
Denver Distribution
P. O. Box 179
Denver, CO 80201
ATTN: Special Projects Program 248

Maxwell Laboratories, Inc.
9244 Balboa Avenue
San Diego, CA 92123
ATTN: A. J. Shannon
ATTN: V. Fargo
ATTN: A. N. Rostocker

McDonnell Douglas Corporation
5301 Bolsa Avenue
Huntington Beach, CA 92657
ATTN: J. Moule
ATTN: N. Harris

Physical Dynamics, Inc.
P. O. Box 1069
Berkeley, CA 94701
ATTN: Joseph B. Workman

Physical Sciences, Inc.
607 North Avenue, Door 18
Wakefield, MA 01880
ATTN: Kurt Wray

R & D Associates
P. O. Box 3580
Santa Monica, CA 90403
ATTN: Robert E. Lelevier
ATTN: Forest Gilmore
ATTN: Richard Latter
ATTN: William B. Wright, Jr.

R & D Associates
1815 N. Ft. Myer Drive
11th Floor
Arlington, VA 2209
ATTN: Herbert J. Mitchell

Rand Corporation, The
1700 Main Street
Santa Monica, CA 90406
ATTN: Cullen Crain
ATTN: James Oakley

Science Applications, Inc.
P. O. Box 2351
La Jolla, CA 92038
ATTN: Daniel A. Hamlin
ATTN: D. Sachs
ATTN: E. A. Straker

Space Data Corporation
1331 South 26th Street
Phoenix, AZ 85034
ATTN: Edward F. Allen

Stanford Research Institute
333 Ravenswood Avenue
Menlo Park, CA 94025
ATTN: M. Baron
ATTN: L. L. Cobb
ATTN: Walter G. Chestnut
ATTN: David A. Johnson
ATTN: Charles L. Rino
ATTN: E. J. Fremouw
ATTN: Ray L. Leadabrand

Stanford Research Institute
306 Wyyn Drive, N. W.
Huntsville, AL 35805
ATTN: Dale H. Davis

Technology International Corporation
75 Wiggins Avenue
Bedford, MA 01730
ATTN: W. P. Boquist

TRW Systems Group
One Space Park
Redondo Beach, CA 90278
ATTN: P. H. Katsos
ATTN: J. W. Lowery

Utah State University
Logan, UT 84321
ATTN: C. Wyatt
ATTN: D. Burt
ATTN: Kay Baker
ATTN: Doran Baker

Visidyne, Inc.
19 Third Avenue
North West Industrial Park
Burlington, MA 01803
ATTN: William Reidy
ATTN: Oscar Manley
ATTN: T. C. Degges
ATTN: J. W. Carpenter